



# Growth suppression of ice crystal basal face in the presence of a moderate ice-binding protein does not confer hyperactivity

Maddalena Bayer-Giraldi<sup>a,b,1</sup>, Gen Sazaki<sup>b</sup>, Ken Nagashima<sup>b</sup>, Sepp Kipfstuhl<sup>a</sup>, Dmitry A. Vorontsov<sup>b,c</sup>, and Yoshinori Furukawa<sup>b</sup>

<sup>a</sup>Helmholtz Centre for Polar and Marine Research, Department of Glaciology (Geosciences), Alfred Wegener Institute, 27568 Bremerhaven, Germany; <sup>b</sup>Institute of Low Temperature Science, Laboratory for Phase Transition Dynamics of Ice, Hokkaido University, 060-0819 Sapporo, Japan; and <sup>c</sup>Faculty of Physics, Lobachevsky State University of Nizhny Novgorod, 603950 Nizhny Novgorod, Russia

Edited by Pablo G. Debenedetti, Princeton University, Princeton, NJ, and approved June 14, 2018 (received for review April 30, 2018)

**Ice-binding proteins (IBPs) affect ice crystal growth by attaching to crystal faces. We present the effects on the growth of an ice single crystal caused by an ice-binding protein from the sea ice microalga *Fragilariopsis cylindrus* (*fc*IBP) that is characterized by the widespread domain of unknown function 3494 (DUF3494) and known to cause a moderate freezing point depression (below 1 °C). By the application of interferometry, bright-field microscopy, and fluorescence microscopy, we observed that the *fc*IBP attaches to the basal faces of ice crystals, thereby inhibiting their growth in the *c* direction and resulting in an increase in the effective supercooling with increasing *fc*IBP concentration. In addition, we observed that the *fc*IBP attaches to prism faces and inhibits their growth. In the event that the effective supercooling is small and crystals are faceted, this process causes an emergence of prism faces and suppresses crystal growth in the *a* direction. When the effective supercooling is large and ice crystals have developed into a dendritic shape, the suppression of prism face growth results in thinner dendrite branches, and growth in the *a* direction is accelerated due to enhanced latent heat dissipation. Our observations clearly indicate that the *fc*IBP occupies a separate position in the classification of IBPs due to the fact that it suppresses the growth of basal faces, despite its moderate freezing point depression.**

ice-binding protein | ice crystallization | growth rates | *Fragilariopsis cylindrus* | DUF3494

**I**ce-binding proteins (IBPs) have a prominent position among molecules and particles interacting with ice due to the fact that they are particularly successful in affecting ice crystal growth. Also referred to as antifreeze proteins (AFPs), IBPs have been found in several polar or cold-tolerant organisms (reviewed in ref. 1). These proteins cause, among other effects, a thermal hysteresis (TH; i.e., a shift of the freezing point below the melting point). Based on this activity, two main IBP groups have been identified. At identical protein concentrations, moderate IBPs cause a TH of up to 1 °C, while hyperactive IBPs induce a much stronger freezing point depression. Moreover, the variance of effectiveness becomes evident from morphological changes of the ice crystal (2). For example, at temperatures slightly below the freezing point, ice crystals in the presence of moderate fish IBPs have a bipyramidal shape and grow preferentially along the *c* axis. However, the preferential growth occurs along the *a* axis in the presence of hyperactive IBPs, resulting in planar ice crystals.

The mechanisms by which IBPs inhibit crystal growth and underlying causes of TH activity differences among various protein groups remain unclear. In this regard, several studies have pointed to a match between certain molecules on the ice-binding site (IBS) of the proteins and defined crystallographic faces of the ice crystals, which allow the formation of stable attachment of IBPs to the ice. In contrast, the high effectiveness of hyperactive proteins has been often attributed to their additional

match to the basal face and therefore, their ability to inhibit growth of the crystals along the *c* axis (3, 4).

The ice-binding proteins from the sea ice diatom *Fragilariopsis cylindrus* (*fc*IBPs) belong to the protein family characterized by the “domain of unknown function” 3494 (DUF3494) as the domain is referred to in the Pfam database. This IBP family was described at first with proteins from the snow mold fungus *Typhula ishikariensis* (5) and from a few diatom species (6). It was later identified in several polar organisms, having likely been transported by horizontal gene transfer (7, 8). The DUF3494 IBPs represent today the most widespread of the known IBP families and can be found in bacteria (9–11), diatoms (12, 13), yeast, and other fungi (14–17) among others.

The classification of *fc*IBPs as moderate or hyperactive from properties described for these proteins is challenging. If we apply the classical scheme described above, which considers the link between TH activity, face affinity, and crystal morphology, *fc*IBPs and other DUF3494 IBPs cannot be described as moderate or hyperactive. For example, *fc*IBP11 is known to have a moderate TH activity, but the crystal morphology shows a planar dendritic pattern (18) as is usually attributed to hyperactive IBPs. The peculiarity of this protein family has been mentioned in the description of other DUF3494 IBPs with moderate TH activity (11, 19, 20) and can also be observed in the IBP from the grass *Lolium perenne* (21).

## Significance

**Ice-binding proteins (IBPs) can be considered a prominent example of macromolecules affecting ice growth kinetics. Until now, two groups of IBPs have been described based on their activity as ice growth inhibitors: moderate and hyperactive IBPs. The mechanism underlying these activity differences has not been clarified yet. Although it is commonly believed that hyperactivity is related to growth inhibition of the basal faces of ice crystals, we show that a moderate IBP can also attach to the basal faces and inhibit their growth. Our observations clearly indicate that this moderate IBP occupies a separate position in the classification of IBPs and contribute to our understanding of interaction between macromolecules and ice and more generally, between macromolecules and inorganic crystals.**

Author contributions: M.B.-G., G.S., and Y.F. designed research; M.B.-G. performed research; K.N. contributed new reagents/analytic tools; M.B.-G., G.S., S.K., D.A.V., and Y.F. analyzed data; and M.B.-G., G.S., D.A.V., and Y.F. wrote the paper.

The authors declare no conflict of interest.

This article is a PNAS Direct Submission.

Published under the PNAS license.

<sup>1</sup>To whom correspondence should be addressed. Email: Maddalena.Bayer@awi.de.

This article contains supporting information online at [www.pnas.org/lookup/suppl/doi:10.1073/pnas.1807461115/-DCSupplemental](http://www.pnas.org/lookup/suppl/doi:10.1073/pnas.1807461115/-DCSupplemental).

Published online July 2, 2018.

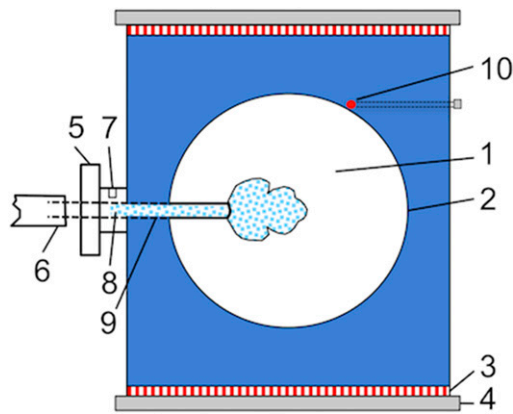


**Fig. 1.** Schematic drawing of the free growth cell with an ice single crystal (highlighted by blue dots) growing from the solution. Details of the setup are given by the inner growth chamber (1) filled with the protein solution, triple-glass windows (2), Peltier elements (3), heat sink (4) with circulating cooling water, capillary holder (5), tube filled with solution (6), inlet for cold shock application (7), the seed crystal formation area (8) located in the glass capillary (9), and the thermistor (10).

However, any data on ice growth kinetics in the presence of *fcIBPs* or any DUF3494 IBP for that matter are entirely missing. Previous publications regarding crystal morphology and growth direction in the presence of DUF3494 IBPs or ice-binding proteins from *L. perenne* (*LpIBPs*) refer to image analyses using only the smallest crystal sizes, around 10–50  $\mu\text{m}$  in diameter (16, 21–23). Although this approach is very helpful for the assessment of protein activity, the usage of small microcrystals does not provide a clear distinction of morphological details and may, therefore, introduce ambiguities in the determination of the orientation of crystallographic axes. Furthermore, experimental factors, like cooling rate and initial crystal size, have been shown to affect the results (24).

In the following, we present a characterization of the growth process of ice single crystals in the presence of *fcIBP11*. We show the morphology and growth rates of ice crystals and the localization of fluorescently labeled *fcIBP11* on the different faces of ice crystals. We interpret our results in the context of growth kinetics and protein activity and question whether *fcIBP11* occupies a separate position in the actual classification of IBPs as moderate or hyperactive proteins.

## Materials and Methods

**The Protein.** We used the IBP isoform 11 from the Antarctic sea-ice diatom *F. cylindrus*, *fcIBP11* (GenBank accession no. DR026070). Previous works on this isoform stressed its relevance as IBP *in vivo*, showing that *fcIBP11* is actively expressed by *F. cylindrus* (6) and suggesting that it plays a role in the diatom as a response to freezing environmental conditions (12), that it binds to ice, and that it has TH activity (18). In this study, we focus on the effect of only one single isoform among the different *fcIBPs* to better understand its interaction with ice from the viewpoint of ice growth physics. Although cooperative effects with other isoforms are important, the elucidation of these effects will be our next challenge in the future after the clarification of the nature of *fcIBP11*. The protein is characterized by the domain classified in the Pfam database as DUF3494 and has a molecular mass of 26 kDa. *fcIBP11* was recombinantly expressed (EMBL Heidelberg) as described in a previous publication (18), whereby the protein solution was diluted and dialyzed in ultrapure water with a resistivity of 18  $\text{M}\Omega\text{-cm}$ . The use of pure water was chosen to focus on the effect of *fcIBP11* on ice, excluding the possible influence of salts on ice crystal growth. Previous experiments had indicated that, at the protein concentrations considered here, the activity of *fcIBP11* is not significantly affected by the absence of a buffer (*SI Appendix, SI Text*). The concentration of the *fcIBP11* solution was limited by the low solubility of the protein in pure water and did not exceed 3  $\mu\text{M}$  (80  $\mu\text{g}/\text{mL}$ ). For fluorescence observations, we used a fusion protein created by recombinantly joining the gene of a fluorescent protein [monomeric Kusabira Orange (mKO)] to the *fcIBP11* gene. The mKO gene was placed at the 5' end of the IBP sequence (GenScript and EMBL Heidelberg). The fusion protein mKO-*fcIBP11* (molecular mass, 50 kDa) was expressed following the protocol for

*fcIBP11* (EMBL Heidelberg), and the protein solution was diluted and dialyzed in ultrapure water. Working solutions had a concentration of 1.6  $\mu\text{M}$  (80  $\mu\text{g}/\text{mL}$ ). The fluorescent mKO protein has an excitation maximum at 548 nm (optimal for excitation with a green laser light) while emitting bright orange light at 559 nm.

**Ice Growth Cell.** We used the same ice growth cell in all measurements in the case of morphology and growth rates determination as well as for fluorescence microscopy. Ice single crystals were grown in a homemade free growth cell filled with the protein solution (Fig. 1). The details of the cell have been explained in detail elsewhere (25). The cell's inner chamber (Fig. 1, 1) was filled with 1 mL of *fcIBP11* solution set to a constant temperature with an accuracy of  $\pm 0.02$   $^{\circ}\text{C}$  using a thermistor (Fig. 1, 10) and two Peltier elements (Fig. 1, 3), one at the top and the other at the bottom of the cell. A thin glass capillary, also filled with the solution (Fig. 1, 9), protruded from outside of the cell into its inner chamber. Rapid freezing was initiated by the injection of a cold spray at the inlet (Fig. 1, 7) to induce the nucleation of ice crystals inside the capillary (Fig. 1, 8). After the formation of many microcrystals, usually only one single crystal reached the tip of the capillary due to geometrical selection and thereafter, was able to expand freely within the supercooled solution inside the chamber. The crystal orientation was adjusted for optimal visualization by rotating the capillary holder (Fig. 1, 5); an example is shown in *SI Appendix, SI Text*. The experiment was halted when growing ice reached the walls of the inner chamber. This moment was determined by monitoring for a temperature increase due to the release of latent heat. The temperature was then set to 5  $^{\circ}\text{C}$  until all ice was melted. At least three runs were made for each experimental condition.

**Morphology and Growth Rates.** To determine the morphology of ice single crystals as well as ice growth rates along the *a* and *c* axes, the free growth cell was set in a microscopic device that combined ordinary bright-field microscopy with Mach-Zehnder interferometry.

Bright-field microscopy was applied to determine the growth rates along the *a* axis by measuring the displacement of the dendrite's tips over time (Fig. 2A) as described previously by Vorontsov et al. (26). The growth rates of the basal faces growing in the *c* direction were measured by Mach-Zehnder interferometry. We used a red laser beam of 670-nm wavelength and 5-mW power. The laser beam, which passed through the sample mostly perpendicular to the basal face, created interference patterns recorded by a CCD camera (Fig.

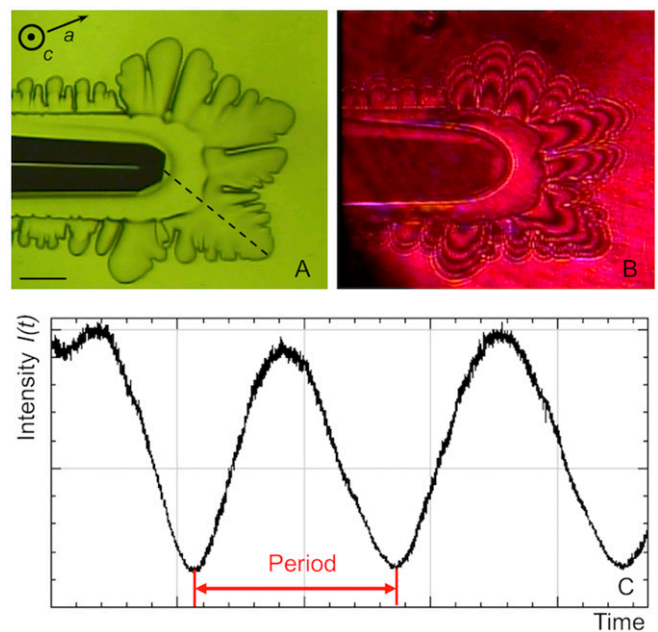


**Fig. 2.** An ice single crystal visualized simultaneously by bright-field microscopy (A) and Mach-Zehnder interferometry (B). The typical interference fringes are visible in B. The direction of observation is perpendicular to the basal face. The movement of the fringes over time is detected with the variation of signal intensity  $I(t)$  measured at selected points on the basal face (C). One period equals the time between the passage of two subsequent fringes and corresponds to a change in ice crystal thickness of 26.9  $\mu\text{m}$ . (Scale bar: 200  $\mu\text{m}$ .)



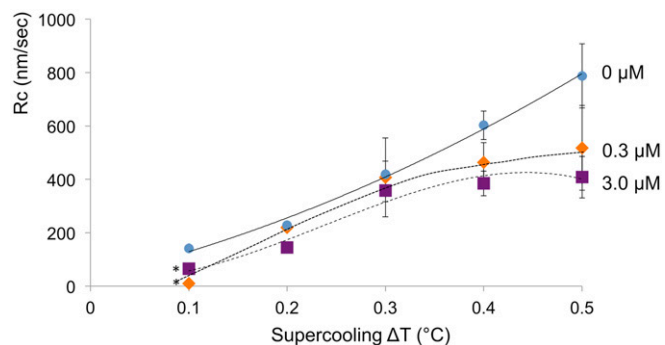


**Fig. 4.** Growth rates  $R_c$  of ice crystals in the  $c$  direction as a function of supercooling at  $fcIBP11$  concentrations of 0, 0.3, and 3.0  $\mu\text{M}$ . The data represent the average of sample size  $n = 3$ , except where indicated. Error bars represent the SD. Trend lines were drawn by hand; \*,  $n = 2$ .

increasing  $fcIBP11$  concentration and is, therefore, consistent with the morphological observations of growth suppression along the  $c$  axis described above (Fig. 3 *D*, *G*, and *J*). The growth of ice in the  $a$  direction was suppressed at low supercoolings ( $\Delta T = 0.1$  °C to 0.3 °C and  $\Delta T = 0.1$  °C in 0.3 and 1.5  $\mu\text{M}$   $fcIBP11$  solutions, respectively) (Fig. 5). When supercooling exceeded these values, crystal growth along the  $a$  axis became faster than in pure water. In contrast, the proteins enhanced ice growth in the  $a$  direction irrespective of the supercooling at  $fcIBP11$  concentration of 3  $\mu\text{M}$ .

**Fluorescence Analysis.** Laser confocal fluorescence microscopy showed the localization of the mKO- $fcIBP11$  molecules on different faces of an ice crystal. Before observation by fluorescence microscopy, we tested mKO- $fcIBP11$  using bright-field microscopy and confirmed that it caused the formation of similar ice crystal shapes like  $fcIBP11$ , indicating that  $fcIBP11$  and mKO- $fcIBP11$  have comparable affinities for ice crystal faces.

Depicted in Fig. 6 are the laser confocal fluorescence microscopy images of growing ice crystals. The basal face was located in the image plane and in the focal plane (Fig. 6*A*), and as one crystal was tilted by 90°, the basal face was oriented perpendicular to the image plane, with the focal plane set inside the crystal (Fig. 6*B*). Fig. 6, *Lower* represents the fluorescence signal intensities measured in the area marked by red rectangles in Fig. 6, *Upper*. Fluorescence intensity on the basal face was significantly higher than that in the mKO- $fcIBP11$  solution surrounding the ice crystal, which suggests that the mKO- $fcIBP11$  molecules accumulated on the basal face. The fluorescence inside the crystal was lower than at the ice-liquid interfaces or in the bulk solution (Fig. 6*B*).

Finally, we noted that, when the ice crystal growth was stopped and the crystal was neither growing nor melting (Fig. 7), mKO- $fcIBP11$  also became visible on the prism faces, thereby indicating protein adsorption over these faces.

## Discussion

**Growth Kinetics of Ice Crystals.** We show that the morphology of ice crystals strongly depends on supercooling and  $fcIBP11$  concentration.

The shapes of the ice crystals observed in pure water are typical for crystals growing from their melt (27). At low supercooling values ( $\Delta T = 0.1$  °C), the ice crystal has a plate-like shape defined by two flat basal faces and a rounded lateral surface (Fig. 3*A*). With increasing supercooling, a dendritic structure develops on the prism faces due to the morphological instability driven by the diffusion of latent heat. Under these conditions, the basal face is known to be molecularly smooth and to grow layer by layer, exhibiting a much slower growth rate than the rough lateral faces. The growth rates in the  $a$  and  $c$  directions determined in this study agree well with the data previously reported (28).

$fcIBP11$  significantly inhibits the growth rate  $R_c$  of the basal faces in the whole ranges of supercooling and  $fcIBP11$  concentrations examined in this study as shown in Fig. 4. This result strongly suggests that  $fcIBP11$  molecules adsorb on the basal faces. The appearance of macrosteps (Fig. 3 *G* and *I*) and pits (Fig. 3 *E* and *F*) observed on the basal faces can be explained by the retardation of the lateral movement of elementary steps by adsorbed  $fcIBP11$  molecules. An example of the process of the formation of macrosteps in a solution with impurities can be found in Land et al. (29). Note that the decrease in the growth rate of the basal faces with increasing  $fcIBP11$  concentration decreases the amount of latent heat generation, having the effect of increasing the supercooling over the lateral faces.

The effects of  $fcIBP11$  on the growth of the prism faces exhibit more complicated results than those on the basal faces (Figs. 3 and 5). When the  $fcIBP11$  concentration is low (0.3  $\mu\text{M}$ ), the crystal has a hexagonal shape (Fig. 3*D*) at a supercooling of 0.1 °C. The growth rate  $R_a$  is lower than in pure water. This result clearly shows that  $fcIBP11$  molecules adsorb on the prism faces and suppress their growth. In contrast, at higher supercooling ( $\Delta T \geq 0.3$  °C), the ice crystals exhibit a dendritic shape induced by morphological instability (Fig. 3 *E* and *F*), and  $R_a$  is accelerated beyond that of pure water. When the  $fcIBP11$  concentration is higher (1.5 and 3.0  $\mu\text{M}$ ), the ice crystals exhibit a dendritic shape bounded by facets (prism faces), as evident in Fig. 3 *G* and *J*, and accelerated growth rates  $R_a$ , even at  $\Delta T < 0.3$  °C. This phenomenon can be explained by taking into account the following two processes: morphological changes of the ice crystal by  $fcIBP11$  and the release of latent heat by the growing ice crystal. The mass growth rate of an ice crystal is determined by the balance between the production of latent heat and its dissipation. The tips of the dendritic crystal branches become sharper with increasing protein concentration, as shown in Fig. 3, due to the fact that the growth of the lateral faces of the dendrite branches, which correspond to the prism faces adsorbed by  $fcIBP11$ , is suppressed. Consequently, the linear growth rate at the dendrite tip may be increased to compensate for the depression of latent heat release that occurs by the reduced growth of the lateral faces. Since the growth rate  $R_c$  of the basal faces was also reduced by attachment of  $fcIBP11$ , the growth rate  $R_a$  at the dendrites tips may be further increased. We conclude that the formation of faceted dendrites observed in the supercooled solution of  $fcIBP11$  is caused by the anisotropic adsorption of this protein on the crystal surface.

The attachment of  $fcIBP11$  to the basal and prism faces was further confirmed by laser confocal fluorescence microscopy. Fig. 6 shows an accumulation of fluorescent protein on the basal face of the ice crystal, which can be caused by different processes such as strong and permanent protein attachment to the basal plane,

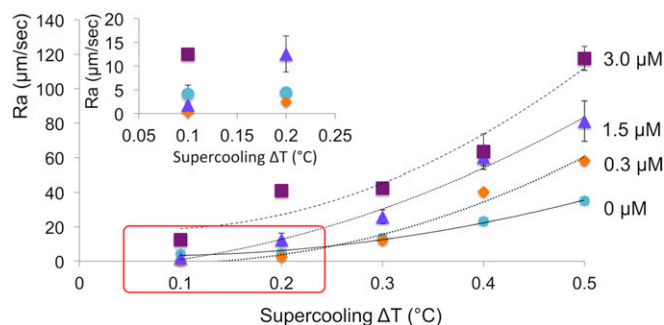


**Fig. 5.** Growth rates  $R_a$  of ice crystals in the  $a$  direction as a function of supercooling at  $fcIBP11$  concentrations of 0, 0.3, 1.5, and 3.0  $\mu\text{M}$ . The data represent the average of sample size  $n = 3$ . The error bars represent the SD. Trend lines were drawn by hand. *Inset* shows a magnification of the area marked by the red rectangle.

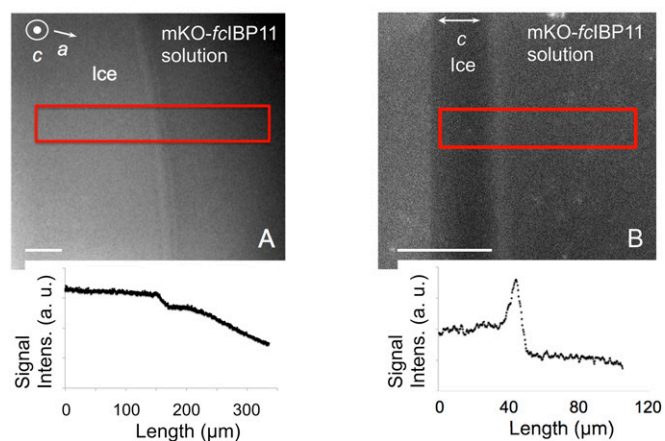


**Fig. 6.** Fluorescence confocal microscopy images of a growing ice crystal in an mKO-*fc*IBP11 solution (1.5  $\mu\text{M}$ ). The basal face is oriented parallel (A) and perpendicular (B) to the observation plane. Lower shows the fluorescence intensities measured in the area marked by the red rectangles. (Scale bar: 50  $\mu\text{m}$ .)

loose and reversible attachment, or rejection of the protein from the growing ice surface. However, we still detect a fluorescence signal on the basal face in Fig. 7, which shows a crystal that is not growing. Therefore, we can conclude that the signal is not caused by rejected mKO-*fc*IBP11, since the molecules would have diffused away in the absence of crystal growth, not resulting in any specific signal over the basal face. Instead, our results indicate attachment of mKO-*fc*IBP11 or at least of a part of it to the basal face. With regard to the prism faces, when the ice crystal is growing (Fig. 6), exposure time of the ice surface to the protein solution is relatively short, and mKO-*fc*IBP11 molecules cannot accumulate on the surface of the prism faces in an amount significant enough to produce a detectable fluorescence signal. However, when crystal growth is halted (and hence, exposure time increased) (Fig. 7), we see mKO-*fc*IBP11 accumulation on the prism faces. We, therefore, conclude that the fluorescence signal is a result of mKO-*fc*IBP11 molecules attaching to the ice surface.

The absence of a fluorescence signal from inside the ice crystal (Fig. 6B) can be explained by a low concentration of mKO-*fc*IBP11 or by a conformation change of the mKO protein caused by its contact with ice. Both cases are conceivable. IBPs have been shown to be attached to ice strongly and irreversibly (30–32), resulting in inclusion within the ice, while other IBPs display a reversible binding mode with detachment of the protein from the crystal surface on ice growth (33, 34). Also, fluorescence can react in different ways to inclusion inside a crystal and can be either maintained (35) or lost (36). After attachment to ice by *fc*IBP11, a destabilization of the mKO protein engulfed in the crystal can easily result in a reversible or irreversible change of its fluorescent properties. Further studies are needed to elucidate whether mKO-*fc*IBP11 is included in the ice crystal.

The inhibition influence of *fc*IBP11 can be described by the classical Cabrera–Vermilyea model (37) or similar pinning models (38, 39). The proteins adsorbed on the crystal become obstacles for step and surfaces, and the curvature of the ice surface locally increases where the flow percolates through pinned *fc*IBP11 molecules. Step flow and surface growth are reduced and eventually stop when the curvature reaches a critical radius as described by the Gibbs–Thomson equation. The adsorbed *fc*IBP11 molecules act as inhibitors to the growth of the basal and prism surfaces at low supercoolings (between 0.1° C and 0.5° C) (Figs. 4 and 5). In the case of the prism faces, this results in the formation of a ragged surface (instead of rounded interfaces typically observed in pure water) and in polygonized and sharp tips of the dendrites.

Note that some previous studies (28, 40) reported the possibility that IBPs may decrease the free energies of ice–water interfaces, resulting in faster growth kinetics and more pronounced morphological instability. In this study, the effect of *fc*IBP11 on the free energy of ice–water interfaces remains uncertain.

**A Moderate IBP with Affinity to the Basal Face.** IBPs have different effects on the growth of the basal face (an overview is presented in *SI Appendix, Table S2*). Detailed crystal growth analyses were carried out with fish AFGP7-8 (41) and fish AFP III (28). Although attachment of AFGPs to the basal face has been reported (42), results of growth analyses indicate that AFGPs and AFP III enhance crystal growth along the *c* axis, whereas *fc*IBP11 presented here has the opposite effect. The promotion of basal face growth is also displayed by other moderate fish IBPs as shown by morphological observations carried out with the smallest ice crystals observed by light microscopy (43, 44). However, hyperactive IBPs suppress the growth along the *c* axis, and growing crystals display a planar dendritic pattern (2). The DUF3494 IBP family is composed of several proteins: some moderate and others hyperactive. Different activities are sometimes displayed by the various isoforms of the same organism, despite high structural similarity (23). However, irrespective of the activity of the protein, ice crystals in the presence of the wide majority of DUF3494 IBPs grow preferentially along the *a* axis (11, 15, 17, 45, 46), and a similar behavior has been described for the *Lp*IBP (21). In the field of IBPs, it has been previously assumed that moderate IBPs adsorb only on the lateral surface of the crystals and that hyperactive IBPs adsorb also on the basal faces. The ability to suppress or restrict crystal growth of the basal face has been repeatedly mentioned as the basis for hyperactivity (1, 3, 45, 47–49). Our study clearly shows that *fc*IBP11 adsorbs on both basal and prism faces of ice crystals and thereby, inhibits growth along the *c* axis, similar to hyperactive IBPs. However, *fc*IBP11 is characterized by a moderate TH activity, similar to that of several DUF3494 IBPs (5, 11, 17, 18, 50). Hence, we can conclude that *fc*IBP11 (and presumably, several other DUF3494 IBPs) should occupy a separate position in the wide spectrum of IBPs. We show that the suppression of growth of the basal face is necessary, but not sufficient, for hyperactivity. A few structural studies have highlighted the role of hydrophobicity of the IBS of DUF3494 IBPs and the relevance of its geometrical match to the ice surface for conferring hyperactivity to the proteins (10, 23, 45). We suggest that the binding of *fc*IBP11 on ice crystal surfaces is much weaker than that of hyperactive IBPs (i.e., the binding energy of IBPs on ice crystal surfaces plays an important role in exhibiting hyperactive TH activity).

The natural environment of *fc*IBP11 is within sea ice brine inclusions, and the icy surface of these inclusions is dominated by the basal face (51). It seems, therefore, of crucial relevance that *fc*IBP11

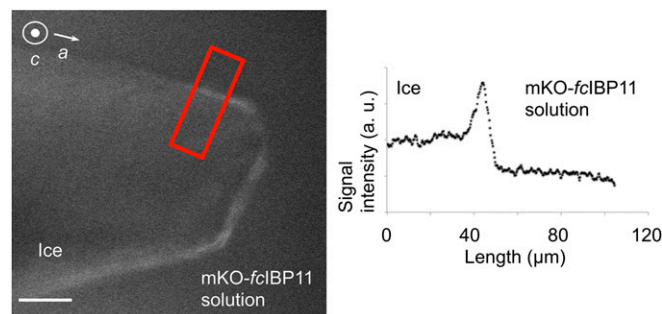


**Fig. 7.** Fluorescence confocal microscopy image of an ice single crystal in an mKO-*fc*IBP11 solution (1.5  $\mu\text{M}$ ) when ice crystal growth was halted. Right shows the fluorescence signal intensity measured in the area marked by the red rectangle. (Scale bar: 50  $\mu\text{m}$ .)

can attach to these planes (*SI Appendix, SI Text*). It is conceivable that *fcIBP11s*, secreted by the diatom cells, bind to the surface of the ice crystals enclosing the brine and affect their growth and morphology, increasing the habitability of the ice and possibly altering the physical properties and biogeochemical imprint (52, 53).

## Conclusions

We have observed that *fcIBP11* induces significant modifications to the shapes of both bulk ice crystals and dendrites. Furthermore, *fcIBP11* also affects the crystal growth rates  $R_a$  and  $R_c$ . This is manifested as reduced growth rates  $R_c$  with increasing protein concentration and supercooling and as faceted ice crystals with reduced ice growth rates  $R_a$  in the  $a$  direction or dendritic forms with increased  $R_a$ , depending on the protein concentration and on supercooling. We conclude that *fcIBP11* molecules attach to both the basal and prism faces as supported by microscopy observations with fluorescent mKO-*fcIBP11* molecules.

The protein's effect on crystal growth rates  $R_a$  can be explained by the morphological changes induced by *fcIBP11* and their resulting effects on the balance between the production and the dissipation of latent heat. We speculate that the affinity of *fcIBP11* for multiple crystal faces, including the basal face, is of crucial importance for survival within sea ice brine (where the basal face is dominant at the interface between ice and brine) and that the proteins actively shape the structure of their icy habitat. Finally, our observations clearly indicate that the basal plane affinity and reduction of growth of the basal face are not sufficient to explain the hyperactivity of IBPs.

**ACKNOWLEDGMENTS.** We acknowledge support from Deutsche Forschungsgemeinschaft SPP1158 (German Research Association Special Program 1158) Grant BA 3694/2-1, Japan Society for the Promotion of Science Invitational Fellowships PE16746 and L17515 and Kakenhi Grant 16K13672, and Hokkaido University.

- Bar Dolev M, Braslavsky I, Davies PL (2016) Ice-binding proteins and their function. *Annu Rev Biochem* 85:515–542.
- Bar-Dolev M, Celik Y, Wettlaufer JS, Davies PL, Braslavsky I (2012) New insights into ice growth and melting modifications by antifreeze proteins. *J R Soc Interface* 9: 3249–3259.
- Scotter AJ, et al. (2006) The basis for hyperactivity of antifreeze proteins. *Cryobiology* 53:229–239.
- Pertaya N, Marshall CB, Celik Y, Davies PL, Braslavsky I (2008) Direct visualization of spruce budworm antifreeze protein interacting with ice crystals: Basal plane affinity confers hyperactivity. *Biophys J* 95:333–341.
- Hoshino T, et al. (2003) Antifreeze proteins from snow mold fungi. *Can J Bot* 81: 1175–1181.
- Janech MG, Krell A, Mock T, Kang J-S, Raymond JA (2006) Ice-binding proteins from sea ice diatoms (Bacillariophyceae). *J Phycol* 42:410–416.
- Sorhannus U (2011) Evolution of antifreeze protein genes in the diatom genus *fragilariopsis*: Evidence for horizontal gene transfer, gene duplication and episodic diversifying selection. *Evol Bioinform Online* 7:279–289.
- Raymond JA, Kim HJ (2012) Possible role of horizontal gene transfer in the colonization of sea ice by algae. *PLoS One* 7:e35968.
- Raymond JA, Fritsen C, Shen K (2007) An ice-binding protein from an Antarctic sea ice bacterium. *FEMS Microbiol Ecol* 61:214–221.
- Do H, Kim S-J, Kim HJ, Lee JH (2014) Structure-based characterization and antifreeze properties of a hyperactive ice-binding protein from the Antarctic bacterium *Flavobacterium frigidum* PS1. *Acta Crystallogr D Biol Crystallogr* 70:1061–1073.
- Mangiagalli M, et al. (2017) Cryo-protective effect of an ice-binding protein derived from Antarctic bacteria. *FEBS J* 284:163–177, and erratum (2017) 284:831.
- Bayer-Giraldi M, Uhlig C, John U, Mock T, Valentin K (2010) Antifreeze proteins in polar sea ice diatoms: Diversity and gene expression in the genus *Fragilariopsis*. *Environ Microbiol* 12:1041–1052.
- Gwak IG, Jung WS, Kim HJ, Kang SH, Jin E (2010) Antifreeze protein in Antarctic marine diatom, *Chaetoceros neogracile*. *Mar Biotechnol (NY)* 12:630–639.
- Raymond JA, Janech MG (2009) Ice-binding proteins from enoki and shiitake mushrooms. *Cryobiology* 58:151–156.
- Xiao N, et al. (2010) Comparison of functional properties of two fungal antifreeze proteins from *Antarctomyces psychrotrophicus* and *Typhula ishikariensis*. *FEBS J* 277:394–403.
- Lee JK, et al. (2010) An extracellular ice-binding glycoprotein from an Arctic psychrophilic yeast. *Cryobiology* 60:222–228.
- Hashim NHF, et al. (2013) Characterization of *Afp1*, an antifreeze protein from the psychrophilic yeast *Glaciozyma antarctica* P112. *Extremophiles* 17:63–73.
- Bayer-Giraldi M, Weikusat I, Besir H, Dieckmann G (2011) Characterization of an antifreeze protein from the polar diatom *Fragilariopsis cylindrus* and its relevance in sea ice. *Cryobiology* 63:210–219.
- Kondo H, et al. (2012) Ice-binding site of snow mold fungus antifreeze protein deviates from structural regularity and high conservation. *Proc Natl Acad Sci USA* 109:9360–9365.
- Park KS, et al. (2012) Characterization of the ice-binding protein from Arctic yeast *Leucosporidium* sp. AY30. *Cryobiology* 64:286–296.
- Middleton AJ, et al. (2012) Antifreeze protein from freeze-tolerant grass has a beta-roll fold with an irregularly structured ice-binding site. *J Mol Biol* 416:713–724.
- Xiao N, et al. (2014) Annealing condition influences thermal hysteresis of fungal type ice-binding proteins. *Cryobiology* 68:159–161.
- Cheng J, Hanada Y, Miura A, Tsuda S, Kondo H (2016) Hydrophobic ice-binding sites confer hyperactivity of an antifreeze protein from a snow mold fungus. *Biochem J* 473:4011–4026.
- Takamichi M, Nishimiya Y, Miura A, Tsuda S (2007) Effect of annealing time of an ice crystal on the activity of type III antifreeze protein. *FEBS J* 274:6469–6476.
- Zepeda S, Nakatsubo S, Furukawa Y (2009) Apparatus for single ice crystal growth from the melt. *Rev Sci Instrum* 80:115102.
- Vorontsov DA, Sazaki G, Hyon S-H, Matsumura K, Furukawa Y (2014) Antifreeze effect of carboxylated  $\epsilon$ -poly-L-lysine on the growth kinetics of ice crystals. *J Phys Chem B* 118:10240–10249.
- Jackson KA (2010) *Kinetic Processes: Crystal Growth, Diffusion, and Phase Transitions in Materials* (Wiley-VCH Verlag GmbH & Co KGaA, Weinheim, Germany).
- Vorontsov DA, et al. (2018) Growth of ice crystals in the presence of type III antifreeze protein. *Cryst Growth Des* 18:2563–2571.
- Land TA, Martin TL, Potapenko S, Palmore GT, De Yoreo JJ (1999) Recovery of surfaces from impurity poisoning during crystal growth. *Nature* 399:442–445.
- Celik Y, et al. (2013) Microfluidic experiments reveal that antifreeze proteins bound to ice crystals suffice to prevent their growth. *Proc Natl Acad Sci USA* 110:1309–1314.
- Drori R, Davies PL, Braslavsky I (2015) When are antifreeze proteins in solution essential for ice growth inhibition? *Langmuir* 31:5805–5811.
- Hudait A, Odendahl N, Qiu Y, Paesani F, Molinero V (2018) Ice-nucleating and antifreeze proteins recognize ice through a diversity of anchored clathrate and ice-like motifs. *J Am Chem Soc* 140:4905–4912.
- Zepeda S, Yokoyama E, Uda Y, Katagiri C, Furukawa Y (2008) In situ observation of antifreeze glycoprotein kinetics at the ice interface reveals a two-step reversible adsorption mechanism. *Cryst Growth Des* 8:3666–3672.
- Mochizuki K, Molinero V (2018) Antifreeze glycoproteins bind reversibly to ice via hydrophobic groups. *J Am Chem Soc* 140:4803–4811.
- Kurimoto M, et al. (2000) Intra-sectoral zoning of proteins and nucleotides in simple crystalline hosts. *Morphology and Dynamics of Crystal Surfaces in Complex Molecular Systems*, MRS Proceedings, eds De Yoreo J, Casey W, Malkin A, Vlieg E, Ward M, Vol 620, p M9.8.1 Cambridge Univ Press, Cambridge, UK.
- Bhatnagar BS, Bogner RH, Pikal MJ (2007) Protein stability during freezing: Separation of stresses and mechanisms of protein stabilization. *Pharm Dev Technol* 12:505–523.
- Cabrera N, Vermilyea DA (1958) The growth of crystals from solution. *Growth and Perfection of Crystals*, eds Doremus RH, Roberts BW, Turnbull D (Wiley, New York), pp 393–410.
- Sander LM, Tkachenko AV (2004) Kinetic pinning and biological antifreezes. *Phys Rev Lett* 93:128102.
- Kubota N (2001) Effect of impurities on the growth kinetics of crystals. *Cryst Res Technol* 36:749–769.
- Kutschan B, Morawetz K, Thoms S (2014) Dynamical mechanism of antifreeze proteins to prevent ice growth. *Phys Rev E Stat Nonlin Soft Matter Phys* 90:022711.
- Furukawa Y, et al. (2017) Oscillations and accelerations of ice crystal growth rates in microgravity in presence of antifreeze glycoprotein impurity in supercooled water. *Sci Rep* 7:43157.
- Wilson PW, Beaglehole D, Devries AL (1993) Antifreeze glycopeptide adsorption on single crystal ice surfaces using ellipsometry. *Biophys J* 64:1878–1884.
- Chao H, DeLuca CI, Davies PL (1995) Mixing antifreeze protein types changes ice crystal morphology without affecting antifreeze activity. *FEBS Lett* 357:183–186.
- Gauthier SY, et al. (2008) A re-evaluation of the role of type IV antifreeze protein. *Cryobiology* 57:292–296.
- Hanada Y, Nishimiya Y, Miura A, Tsuda S, Kondo H (2014) Hyperactive antifreeze protein from an Antarctic sea ice bacterium *Colwellia* sp. has a compound ice-binding site without repetitive sequences. *FEBS J* 281:3576–3590.
- Kim M, Gwak Y, Jung W, Jin E (2017) Identification and characterization of an isoform antifreeze protein from the Antarctic marine diatom, *Chaetoceros neogracile* and suggestion of the core region. *Mar Drugs* 15:E318.
- Graether SP, et al. (2000) Beta-helix structure and ice-binding properties of a hyperactive antifreeze protein from an insect. *Nature* 406:325–328.
- Jia Z, Davies PL (2002) Antifreeze proteins: An unusual receptor-ligand interaction. *Trends Biochem Sci* 27:101–106.
- Davies PL (2014) Ice-binding proteins: A remarkable diversity of structures for stopping and starting ice growth. *Trends Biochem Sci* 39:548–555.
- Lee JH, et al. (2012) Structural basis for antifreeze activity of ice-binding protein from arctic yeast. *J Biol Chem* 287:11460–11468.
- Thomas DN, Dieckmann GS (2010) *Sea Ice* (Wiley-Blackwell, Hoboken, NJ), 2nd Ed.
- Raymond JA (2011) Algal ice-binding proteins change the structure of sea ice. *Proc Natl Acad Sci USA* 108:E198.
- Krembs C, Eicken H, Deming JW (2011) Exopolymer alteration of physical properties of sea ice and implications for ice habitability and biogeochemistry in a warmer Arctic. *Proc Natl Acad Sci USA* 108:3653–3658.